First-order topological phase transition of the Haldane-Hubbard model

Jakub Imriška,[1] Lei Wang,[1,2] and Matthias Troyer[1]
[1]*Theoretische Physik, ETH Zurich, 8093 Zurich, Switzerland*
[2]*Beijing National Laboratory for Condensed Matter Physics, and Institute of Physics, Chinese Academy of Sciences, Beijing 100190, China*
(Received 18 April 2016; published 5 July 2016)

We study the interplay of topological band structure and conventional magnetic long-range order in spinful Haldane model with on-site repulsive interaction. Using the dynamical cluster approximation with clusters of up to 24 sites we find evidence of a first-order phase transition from a Chern insulator at weak coupling to a topologically trivial antiferromagnetic insulator at strong coupling. These results call into question a previously found intermediate state with coexisting topological character and antiferromagnetic long-range order. Experimentally measurable signatures of the first-order transition include hysteretic behavior of the double occupancy, single-particle excitation gap, and nearest neighbor spin-spin correlations. This first-order transition is contrasted with a continuous phase transition from the conventional band insulator to the antiferromagnetic insulator in the ionic Hubbard model on the honeycomb lattice.

DOI: 10.1103/PhysRevB.94.035109

I. INTRODUCTION

The Haldane model [1] describes noninteracting fermions on a honeycomb lattice in a staggered magnetic field. Over the past decade, this prototypical model of a topologically nontrivial band structure has inspired numerous developments in the field of topological insulators [2,3], and has recently been experimentally realized using ultracold fermions in an optical lattice [4]. Because of their high degree of controllability, ultracold atomic gases offer a unique opportunity to investigate the interplay of topological band structure and the strong interactions, where one expects a variety of fascinating phenomena [5].

To experimentally investigate the interaction effects on the Haldane model, one loads two species of ultracold fermionic atoms into an optical lattice and tunes their on-site interaction. However, the Haldane-Hubbard model poses a theoretical challenge. The lack of time-reversal symmetry gives rise to a severe fermion sign problem [6] and limits the use of quantum Monte Carlo (QMC) methods [7]. This is in contrast with the time-reversal symmetric Kane-Mele-Hubbard (KMH) model, in which the two spin species experience opposite magnetic flux. The KMH model thus allows sign-problem free QMC simulations at half filling that show a continuous phase transition from the quantum spin Hall insulator into an antiferromagnetic insulator (AFI) as the interaction strength increases [8–10].

Similarly, in the Haldane-Hubbard model the local onsite interaction favors an AFI in the strong coupling regime [11,12], which competes with a Chern insulator (CI) at weak coupling. To find out how the two limiting cases are connected requires a nonperturbative treatment. Being hard to tackle, some of the previous studies used static mean-field approximations [13–17]. All these studies reported an additional phase with coexisting antiferromagnetic long-range order and nontrivial topological character at intermediate interaction strengths. This topologically nontrivial AFI state has a clear mean-field picture: in the vicinity of a putative second-order quantum phase transition to the AFI, the antiferromagnetic order parameter increases continuously so that there is a finite region where the topological band gap persists despite of the counteracting topologically trivial band gap due to the magnetic order. However, given the approximate nature of the static mean-field treatment, it is hard to assess whether this intermediate state really exists.

In this paper we thus study the ground state phase diagram of the Haldane-Hubbard model using the dynamical cluster approximation (DCA) [18,19], which is a cluster extension of dynamical mean-field theory (DMFT) [20]. By using clusters embedded in a self-consistently determined bath, both short-range correlations within the cluster and long-range correlations are captured. Solving embedded clusters with up to 24 sites at low temperature we can go beyond static mean-field treatments, exact diagonalization, and previous small cluster studies [35,42,43]. As the latter are not consistent, a larger cluster study with reduced approximation bias is required for reliable statements. Our main result is a *first-order* phase transition from a topologically nontrivial band insulating state to a magnetic long-range ordered state, preempting the intermediate "topological AFI" state. Observables such as the antiferromagnetic magnetization, double occupancy, all exhibit hysteretic behavior around the transition point, which are clear signatures of a first-order phase transition [21].

A similar transition between a Mott insulator and a quantum spin Hall insulator was found in the Bernevig-Hughes-Zhang-Hubbard model using DMFT with suppressed long-range order [22,23].

II. MODEL AND METHOD

The Hamiltonian of the Haldane-Hubbard model reads

$$\hat{H} = -t \sum_{\langle i,j\rangle,\sigma} \hat{c}^{\dagger}_{i\sigma}\hat{c}_{j\sigma} - \mathrm{i}\lambda \sum_{\langle\langle i,j\rangle\rangle,\sigma} v_{ij}\hat{c}^{\dagger}_{i\sigma}\hat{c}_{j\sigma} + \Delta \sum_{i,\sigma} s_i \hat{n}_{i\sigma} + U \sum_i \left(\hat{n}_{i\uparrow} - \frac{1}{2}\right)\left(\hat{n}_{i\downarrow} - \frac{1}{2}\right), \quad (1)$$

where $\hat{c}^{\dagger}_{i\sigma}$ ($\hat{c}_{i\sigma}$) creates (annihilates) a fermion at site i of the honeycomb lattice with spin $\sigma \in \{\uparrow,\downarrow\}$, $\hat{n}_{i\sigma} \equiv \hat{c}^{\dagger}_{i\sigma}\hat{c}_{i\sigma}$ denotes the occupation number operator, t is the hopping amplitude between nearest neighbors $\langle i,j\rangle$, and $\mathrm{i}\lambda$ is the purely imaginary

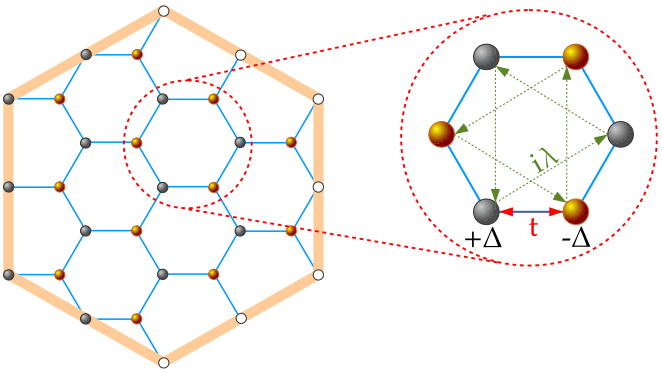

FIG. 1. Embedded cluster with 24 sites used to obtain the phase diagram. White sites on the border correspond via periodic boundary conditions to gray sites on the opposite border. The enlarged hexagon shows the terms of the noninteracting part of the Hamiltonian Eq. (1): nearest neighbor hopping t, next nearest neighbor hopping $i\lambda$, and staggered potential, which is $+\Delta$ $(-\Delta)$ on the sublattice with orange (gray) sites.

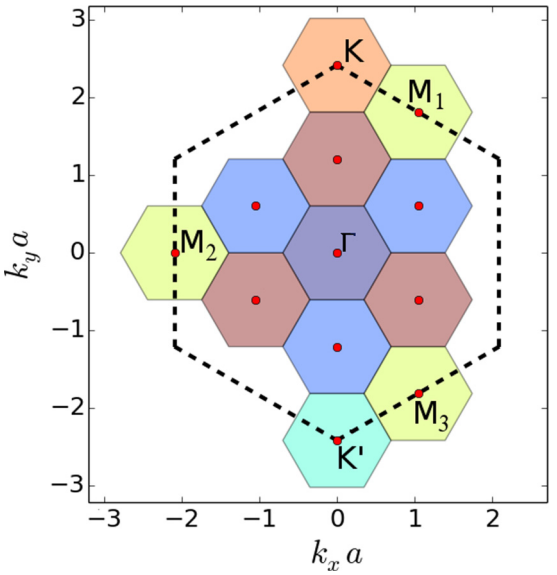

FIG. 2. DCA patches in the reciprocal space for the 24-site cluster used throughout the study. The number of DCA patches, 12, equals the number of unit cells contained by the cluster. The Brillouin zone of the lattice is the interior of the dashed hexagon. All high symmetry points of the Brillouin zone, Γ, K, K', and the three "time-reversal symmetric" points M_i, are located at a patch center. The nearest neighbor distance of sites in real space is denoted by a.

hopping between next-nearest-neighbor sites $\langle\langle i,j\rangle\rangle$. $v_{ij} = -1\,(+1)$ for the hopping from site i to j in (counter-)clockwise direction with respect to the center of the hexagon, illustrated in Fig. 1. The sign s_i is $+1$ on one sublattice of the honeycomb lattice and -1 on the other. The last term is the on-site repulsive interaction with strength $U > 0$. Without loss of generality we assume $\lambda \geqslant 0$.

The main focus of our study is the half-filled Haldane-Hubbard model with $\lambda \neq 0$ and $\Delta = 0$. Without interactions ($U = 0$), the ground state is a topologically nontrivial Chern insulator (CI) with Chern number 1 for both spin species and a band gap $\min(\sqrt{27}\lambda, t)$. For comparison, we also consider the ionic Hubbard model on the honeycomb lattice with staggered chemical potential $\Delta \neq 0$ and $\lambda = 0$. In this case the noninteracting system also has a finite band gap, determined by Δ, but it is topologically trivial. The full model (1) can be experimentally implemented with independent tunability of each term [4,24].

To map out the ground state phase diagram of Eq. (1) using the DCA method [18,19], we solve a cluster impurity problem embedded self-consistently into a bath using continuous-time auxiliary-field QMC method with submatrix updates [25,26]. DCA approximates the lattice self-energy as a patchwise constant function equal to the impurity self-energy at the cluster reciprocal point in the center of each patch. In the limit of infinite cluster size the approximation yields exact results. Details of the DCA method for multisite unit cells are described in Ref. [27]. For most of this study we use the cluster shown in Fig. 1, which respects the threefold rotational symmetry of the honeycomb lattice. Its reciprocal representation displayed in Fig. 2 contains all the high symmetry reciprocal lattice points of our model. The noninteracting dispersion of $\hat{H}$ is linear at K and K' only for $\Delta = \lambda = 0$. The K and K' points remain the points of minimal noninteracting band gap for $\lambda/t \leqslant 1/\sqrt{27} \approx 0.192$ irrespective of Δ.

For $\lambda = 0$ and $\Delta = 0$, the model reduces to the honeycomb lattice Hubbard model where sign-problem free QMC simulations have shown a continuous phase transition from a Dirac semimetal to an AFI [28,29]. However, the model suffers from a sign problem [6,7] for $\lambda \neq 0$ or $\Delta \neq 0$. Even though the sign problem is mitigated in the DCA approach compared to lattice QMC simulations, it still limits the accessible cluster size, temperature, and parameter ranges of λ or Δ. We perform simulations at a temperature $T/t = 1/16$, which corresponds to the bulk noninteracting gap of the Haldane model at $\lambda/t \approx 0.012$. This temperature is below all relevant energy scales and should thus exhibit ground state behavior of the model. The sign problem limits the accessible range of λ for the chosen cluster and temperature to $\lambda/t \leqslant 0.15$, which nevertheless lies in the experimentally relevant region [4].

To characterize the magnetic properties of the system we measure the staggered magnetization in the cluster

$$m = \frac{1}{N}\sum_i s_i \langle \hat{n}_{i\uparrow} - \hat{n}_{i\downarrow}\rangle, \tag{2}$$

with N being the number of sites of the cluster. While the investigated two-dimensional model cannot spontaneously break the continuous symmetry at nonzero temperature [30,31], the DCA solution at a low but nonzero temperature T may still develop magnetic long-range order as DCA treats long-range correlations in a mean-field fashion. Such ordered solution should be thought of as a DCA approximation of the ground state. By systematically increasing the cluster size the DCA result then becomes increasingly accurate.

To reveal the topological nature of the phase we compute the Chern number, using the topological Hamiltonian of Ref. [32],

$$H_{\text{topo}}(\mathbf{k}) \equiv -G^{-1}(i\omega = 0, \mathbf{k}) = H_0(\mathbf{k}) + \Sigma(i\omega = 0, \mathbf{k}), \tag{3}$$

where $H_0(\mathbf{k})$ is the noninteracting part of the Hamiltonian (1). We obtain $\Sigma(i\omega = 0, \mathbf{K})$ by a cubic spline interpolation

over 40 lowest (positive and negative) Matsubara frequency self-energies $\Sigma(i\omega_n,\mathbf{K})$. In the DCA, the self-energy $\Sigma(\mathbf{k})$ is approximated by the impurity self-energy $\Sigma(\mathbf{K})$ at the closest cluster momentum $\mathbf{K}$, i.e., it is a patchwise constant function in reciprocal space. The Chern number calculation utilizing H_{topo} is performed by discretization of the Brillouin zone as in Ref. [33]. The results are robust with respect to different Brillouin zone discretization meshes. In addition we checked robustness of the results with respect to interpolation of the self-energy in reciprocal space using natural neighbor interpolation. The Chern number, being a topological invariant, may change only if the topological gap, i.e., the band gap of $H_{\text{topo}}(\mathbf{k})$, closes. We find that for all examined values of λ, i.e., for $\lambda/t \leqslant 0.15$, the topological gap closes at the K and K' point [34], while the single particle gap of the physical Hamiltonian (1) remains finite.

III. RESULTS

A. Phase diagram

Figure 3 shows our phase diagram of the Haldane-Hubbard model. For $\lambda/t \geqslant 0.075$, we find clear evidence of a first-order transition from the CI to the topologically trivial AFI shown by the black solid line. This phase boundary is not extrapolated in cluster size. To assess the systematic error, we consider the $\lambda = 0$ limit where the model reduces to the honeycomb lattice Hubbard model where unbiased QMC methods predict a critical interaction to lie between $3.78t$ and $3.9t$ [28,29]. The unextrapolated value $U_{\text{HH}}(\lambda = 0)/t = 3.575 \pm 0.075$ based on our 24-site cluster underestimates this value by about $0.3t$, as the DCA transition occurs when the correlation length reaches the order of the cluster size. This difference provides an estimate of the systematic error. At the first-order transition the systematic error is expected to be smaller as the correlation length there remains finite and the DCA should well describe the lattice properties. For $\lambda/t \leqslant 0.05$ DCA with 24-site cluster is consistent with a continuous phase transition with intermediate topological AFI. However, we believe this to be due to an insufficiently large cluster and that using larger clusters will again lead to a first-order transition.

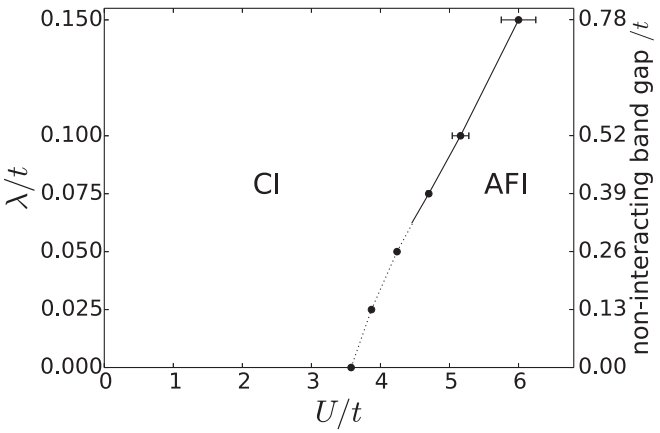

FIG. 3. Phase diagram of the Haldane-Hubbard model on honeycomb lattice based on simulation at $T/t = 1/16$ using the 24-site cluster. The solid line is a first-order phase transition in the Haldane-Hubbard model from the CI to the AFI. On the dotted line we do not have confidence about the character of the transition even though we observe continuous phase transition (see text for discussions). The error bars of the data points indicate the range of the hysteresis. The right vertical axis shows the size of the noninteracting band gap, $\sqrt{27}\lambda$.

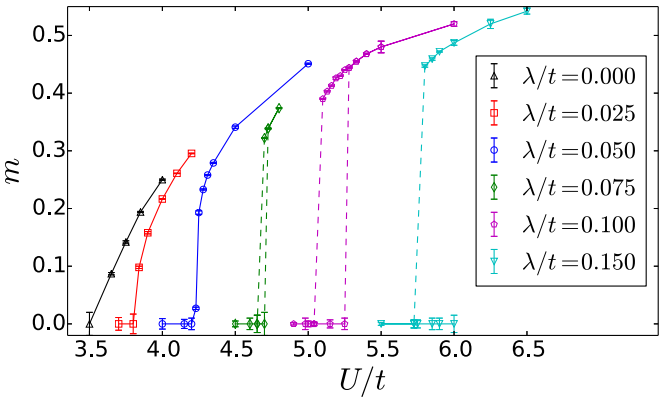

FIG. 4. Staggered magnetization as a function of U/t for different λ/t obtained for a 24-site cluster at $T/t = 1/16$. The dashed lines indicate a discontinuity of the staggered magnetization, and the region between the dashed lines indicates the hysteretic region where it is possible to converge to either a paramagnetic or an antiferromagnetically ordered solution. This hysteresis is visible for $\lambda/t = 0.075$, 0.1, and 0.15. For $\lambda = 0.15t$ we do not provide the upper bound for stability of the paramagnetic phase due to a too large sign problem.

1. *First-order transition for* $\lambda/t \geqslant 0.075$

Figure 4 shows the staggered magnetization as a function of U/t for various values of λ. Noticeably, m shows a discontinuity for $\lambda/t \geqslant 0.075$, accompanied by hysteretic behavior. The simulation can converge to two different solutions depending on the initial bare cluster Green's function provided to the self-consistency loop. This provides a clear signature of a first-order phase transition at $\lambda/t \geqslant 0.075$. In order to distinguish between slow convergence of the self-consistency procedure and (meta)stable solutions we perform about 100 iterations.

Around the first-order transition other observables also exhibit hysteretic behavior, as shown in Fig. 5 for $\lambda/t = 0.1$. The two curves in each panel are obtained with self-consistent iterations started either from the CI or from the AFI state. Hysteretic behavior in these observables can also be measured experimentally as a signature of a first-order phase transition. The single particle gap Δ_{sp} is obtained from the imaginary time lattice Green's function at the K point by fitting to $A\cosh[\Delta_{\text{sp}}(\tau - B)]$ near $\tau = 1/(2T)$. Note that in this case the temperature $T/t = 1/16$ is for all values of U at least four times smaller than the single particle gap, and thus low enough to capture ground state behavior. The average sign of the impurity solver is also notably different in the two phases and exhibits a jump at the transition point. The Chern number (not plotted) equals 1 for the nonmagnetic solutions and 0 for the magnetic solutions.

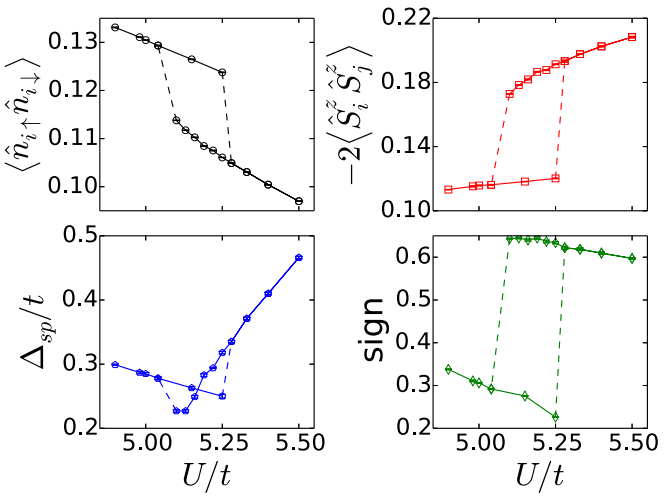

FIG. 5. Double occupancy $\langle \hat{n}_{i\uparrow}\hat{n}_{i\downarrow} \rangle$, nearest neighbor spin-spin correlation function $-2\langle \hat{S}_i^z \hat{S}_j^z \rangle$, single particle gap Δ_{sp}, and the average sign in the simulation are shown as a function of U at $\lambda/t = 0.1$. The dashed line segments show the discontinuity at the first-order phase transition.

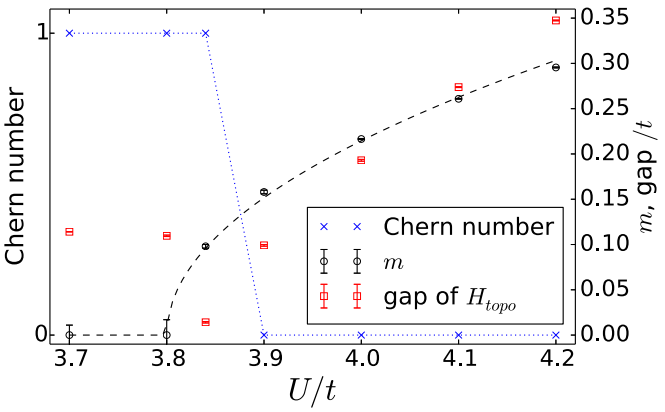

FIG. 6. Staggered magnetization and the topological gap at the K point as a function of U/t for $\lambda/t = 0.025$. The fit of the staggered magnetization in range $U/t \in [3.7,4.1]$ uses the mean-field critical exponent $\beta_{\text{mf}} = 0.5$. The Chern numbers of the occupied bands drop between $3.84 < U/t < 3.9$, consistent with closing of the gap of H_{topo} in the same range. The dotted line is a guide to the eye.

This clear evidence of a first-order phase transition is different than the continuous phase transition transition found in the static mean-field [13–17] and two-site cellular DMFT [35] (CDMFT) studies. Since our DCA calculation on a 24-site cluster incorporates short-range correlation effects and we can reproduce some of the continuous transition character by using small clusters (see Sec. III C), we believe the first-order transition found in the Haldane-Hubbard model is real.

2. *Phase transition for* $\lambda/t < 0.075$

For $\lambda/t \leqslant 0.05$, we find a continuous increase of the staggered magnetization, as shown in Fig. 4. As a consequence of the smooth increase of the magnetic order parameter, an intermediate topologically nontrivial AFI appears in between the CI for low U and the AFI for large U. The simulation results at $\lambda/t = 0.025$ are depicted in terms of the topological gap at the K point, the staggered magnetization m, and the Chern number as a function of U in Fig. 6. The Chern number drops from 1 to 0 inside the magnetic ordered phase. The same scenario is found at $\lambda/t = 0.05$.

Even though our DCA results are consistent with an intermediate topological AFI state in a small region of parameter space, the data is also consistent with the scenario of a first-order phase transition for any nonzero λ, and a diverging correlation length as $\lambda \to 0$. In this scenario, the correlation length at the first-order transition remains finite at any nonzero λ, but is larger than the 24-site cluster employed here, thus resulting in an apparent continuous phase transition for $\lambda/t \leqslant 0.05$ region. Larger clusters would thus be required to resolve the phase transition character in the small λ region, but are intractable because of the sign problem.

Finally, for $\lambda = 0$, the model reduces to the Hubbard model on the honeycomb lattice, where there is a firm evidence that the model undergoes a direct second-order phase transition from the paramagnetic semimetal to the AFI [28,29]. A DCA study of that model predicts in agreement with the latter studies the direct second-order phase transition [36]. In the vicinity of a second-order phase transition the correlation length exceeds the cluster size and then mean-field behavior appears in the DCA solution.

B. Comparison to the ionic Hubbard model on the honeycomb lattice

To obtain more insight into the phase transition between the CI and the AFI in the Hubbard-Haldane model, we compare its phase diagram with that of the ionic Hubbard model on honeycomb lattice. The latter model is defined by $\lambda = 0$ and a staggered sublattice potential $\pm\Delta$, which opens a topologically trivial band gap. The noninteracting dispersion of the Haldane and the ionic models are similar if the noninteracting band gaps are adjusted to match each other. The density of states for both models with noninteracting band gap $0.52t$ is shown in the inset of Fig. 7 [37]. Thus, in a crude theoretical treatment which only cares about the band gap or density of states, these two models should have similar phase diagrams. However, the phase diagram of the ionic honeycomb model shown in Fig. 7 differs substantially from that of the Haldane-Hubbard model in Fig. 3. The dependence of the critical interaction strength on the noninteracting band gap in the ionic model is weaker than in the Haldane-Hubbard model. More importantly, the character of the transition is second order in the ionic Hubbard model for all simulated parameters. The origin of such difference may be due to distinct symmetry (time-reversal symmetry breaking in the Haldane-Hubbard model, inversion symmetry breaking in the ionic model) or topological characters of the two models.

While the ionic Hubbard model on the square lattice exhibits an intermediate metallic phase between the ionic band insulator (BI) and AFI [38–40], our simulations find no indication of such phase on the honeycomb lattice. A reason for this difference may be the different position of the van Hove singularities, which are at the band edges for the square lattice, but not for the honeycomb lattice. A similar observation was made in Ref. [41].

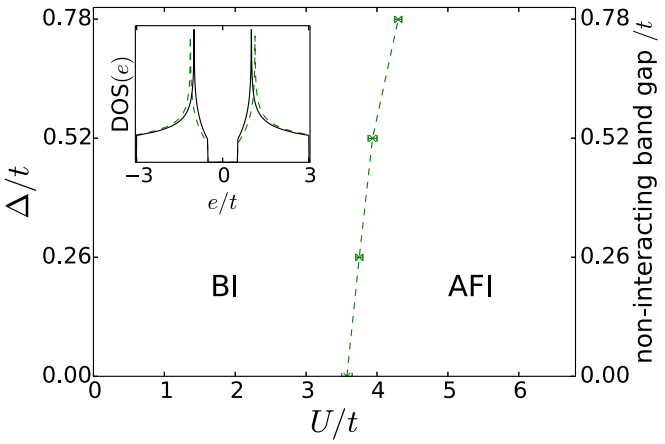

FIG. 7. Phase diagram of the ionic Hubbard model on the honeycomb lattice based on simulations at $T/t = 1/16$. The dashed line denotes the critical interaction strength U_{IH} of a second-order phase transition from a band insulator to an AFI. The error bars show the bounds for the onset of ordering for a 24-site cluster. The inset shows the density of states of the noninteracting Haldane model at $\lambda/t = 0.1$ as a solid black line, and that of the noninteracting ionic model for $\Delta = 0.52t$ as a dashed green line. Both models have a band gap of $0.52t$.

C. Comparison to small cluster calculations

Both static mean-field calculations [13–17] and CDMFT on 2-site clusters [35] predict a continuous phase transition from CI to the AFI, with an intermediate topologically nontrivial AFI phase for a wide range of λ. Also results of a variational cluster approximation calculation on 6-site clusters [35,42] indicate an indirect transition from CI to AFI, but via a topologically nontrivial nonmagnetic insulating phase with opposite Chern number as the CI. Another recent study using 6-site DCA and CDMFT calculations [43] reports, similar to our findings, a signature of a first-order transition for $\lambda/t = 0.2$. Since all studies mentioned above employ quantum cluster approaches of a similar nature, these discrepancies may either be due to insufficiently large clusters or due to subtleties in the cluster embeddings which break the spatial symmetries [44,45].

To shed light on this issue we examined the Haldane-Hubbard model using two additional clusters of different size, shown in Fig. 8. The 6-site cluster contains the K and K' point in its reciprocal representation, while the 8-site cluster does not. Both of them respect the threefold rotational symmetry. The staggered magnetization obtained using these clusters at $\lambda/t = 0.1$ are shown in Fig. 9. The 6-site cluster displays similar hysteresis as observed above for the 24-site cluster, with a difference in the transition point U/t of at most 0.1. The value of m in the ordered phase is larger than for the 24-site cluster, which is expected, as DCA becomes exact for $N \to \infty$ and m has to vanish in the thermodynamic limit at $T \neq 0$. In contrast, using the 8-site cluster we observe a sharp but continuous increase of m at a strongly shifted transition point $U_{\mathrm{HH}}/t = 5.40 \pm 0.03$ for $\lambda/t = 0.1$, without any trace of hysteresis. These findings are similar to those obtained for Haldane model of spinless fermions [46–48], where Varney *et al.*, using exact diagonalization, observed first-order or

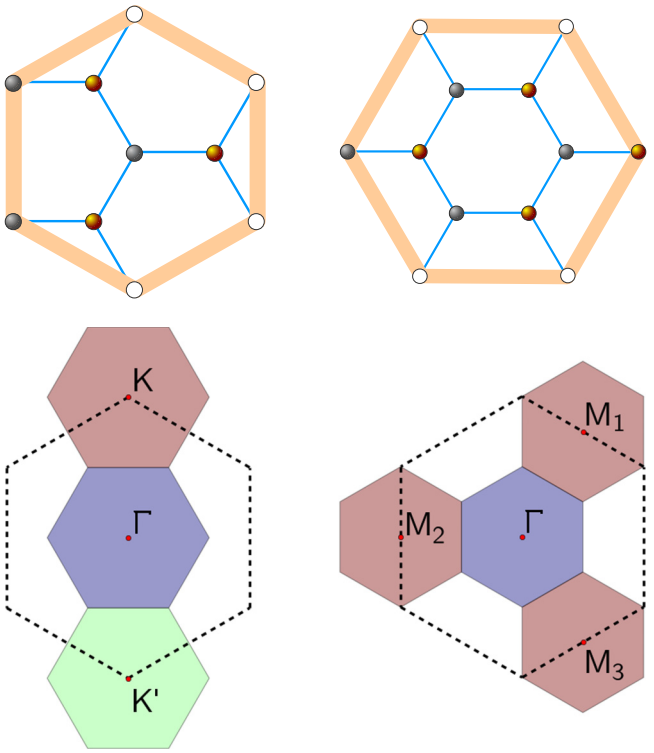

FIG. 8. Top: the 6-site and the 8-site cluster shown in real space. As in Fig. 1, the white sites on the border correspond via periodic boundary conditions to the border sites. Bottom: the DCA patches for the 6-site and the 8-site clusters in reciprocal space. The Brillouin zone of the lattice is the interior of the dashed hexagon. The 6-site cluster contains the K, K' points as patch centers, while the 8-site cluster does not.

continuous transition character depending on the presence of the K and K' points in the cluster reciprocal representation. Our findings in DCA support their conclusion that the choice of the cluster is significant and that reliable clusters need to contain the K and K' points.

Examining the model within the DMFT approximation yields further insight. For this we simulate a single site in

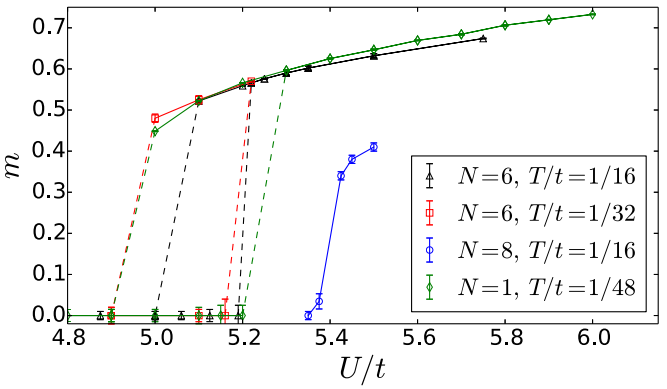

FIG. 9. Staggered magnetization obtained for the Haldane-Hubbard model at $\lambda/t = 0.1$ using additional small clusters shown in Fig. 8 simulated at temperature T. The single-site DMFT data ($N = 1$) is presented as well.

sublattice A. The form of the $\mathbf{k}$-independent DMFT self-energy for a single unit cell (containing two sites) is obtained only from the self-energy of the simulated site. Its form has to respect the symmetry of the studied Hamiltonian 1, which is invariant (up to irrelevant constants) under particle-hole transformation combined with spatial inversion, ensuring

$$G_{AA\sigma}(i\omega_n,\mathbf{k}) = -G^*_{BB\sigma}(i\omega_n,\mathbf{k}), \tag{4}$$

both in the paramagnetic and in the antiferromagnetically ordered phase. The DMFT self-energy is then approximated by

$$\Sigma_{BB\sigma}(i\omega_n) = -\Sigma^*_{AA\sigma}(i\omega_n), \tag{5}$$

$$\Sigma_{AB\sigma}(i\omega_n) = 0 = \Sigma_{BA\sigma}(i\omega_n), \tag{6}$$

neglecting the off-diagonal components, motivated by the dominantly local character of the self-energy for a Hubbard interaction. The DMFT mapping is then formulated conveniently with 2×2 matrices, comprising the sublattice indices,

$$G_{AA\sigma}(i\omega_n) = \frac{1}{\Omega}\int_{\mathrm{BZ}} d\mathbf{k}\left[\left(G^0_\sigma(i\omega_n,\mathbf{k})\right)^{-1} - \Sigma_\sigma(i\omega_n)\right]^{-1}_{AA}, \tag{7}$$

integrating over the Brillouin zone (with volume Ω). Here $G^0_\sigma(i\omega_n,\mathbf{k}) = [i\omega_n\mathbb{1} - H_0(\mathbf{k})]^{-1}$ is the noninteracting lattice Green's function. Surprisingly, the magnetization curve for the Haldane-Hubbard model at $\lambda/t = 0.1$ shows discontinuities and hysteresis (Fig. 9) even in the DMFT simulation. This apparent contradiction to our conclusion about the necessity of the K and K' point in the cluster reciprocal representation can be explained by the prescribed form of the DMFT self-energy in Eqs. (5) and (6), which *coincidentally* obeys the same constraints, of vanishing AB components, as those due to the symmetry of the self-energy at the K and K' point, arising from the threefold rotational symmetry of the model. For the ionic honeycomb model simulated by DMFT at $\Delta/t = 0.52$, m is continuous. Note that the next-nearest neighbor hoppings on the same sublattice ($\lambda \neq 0$) do not allow one to rewrite the mapping Eq. (7) as an integral over the density of states, which explains the possibility of finding qualitatively different behaviors of the magnetization in the Haldane-Hubbard and the ionic honeycomb model despite their very similar noninteracting density of states.

Finally, the 6-site cluster enable simulations at lower temperature since the sign problem is less severe than for the 24-site cluster. Results obtained at twice lower temperature differ only by an enlarged ordered phase (see Fig. 8), while the first-order characteristics remain unchanged.

IV. OUTLOOK

Our predictions can be checked by the experiments on the Haldane-Hubbard model in optical lattice simulators [21,24]. The first-order phase transition can be detected as a hysteresis of spatially averaged local observables. By tuning the interaction strength to the coexisting region one may also find coexisting domains of CI and AFI phases. Each AFI domain is of the size of the magnetic correlation length at the first-order transition point. Interestingly, the topological nature of the CI would imply presence of chiral edge states around the domain walls which may be revealed by an *in situ* measurement of the domains in the ultracold atomic gas.

ACKNOWLEDGMENTS

We thank Emanuel Gull for providing us with the continuous-time auxiliary-field impurity solver for real Hamiltonians [25], which we adapted to handle complex Hamiltonians. We appreciate discussions with Gregor Jotzu and Michael Messer. The code is based on the ALPS libraries [49,50] and calculations were performed on the Mönch cluster. This work was supported by the European Research Council through ERC Advanced Grant SIMCOFE and by the Swiss National Science Foundation through NCCR QSIT.

[1] F. D. M. Haldane, Phys. Rev. Lett. **61**, 2015 (1988).
[2] M. Z. Hasan and C. L. Kane, Rev. Mod. Phys. **82**, 3045 (2010).
[3] X.-L. Qi and S.-C. Zhang, Rev. Mod. Phys. **83**, 1057 (2011).
[4] G. Jotzu, M. Messer, R. Desbuquois, M. Lebrat, T. Uehlinger, D. Greif, and T. Esslinger, Nature (London) **515**, 237 (2014).
[5] M. Hohenadler and F. F. Assaad, J. Phys.: Condens. Matter **25**, 143201 (2013).
[6] E. Y. Loh, J. E. Gubernatis, R. T. Scalettar, S. R. White, D. J. Scalapino, and R. L. Sugar, Phys. Rev. B **41**, 9301 (1990).
[7] M. Troyer and U.-J. Wiese, Phys. Rev. Lett. **94**, 170201 (2005).
[8] M. Hohenadler, T. C. Lang, and F. F. Assaad, Phys. Rev. Lett. **106**, 100403 (2011).
[9] H.-H. Hung, L. Wang, Z.-C. Gu, and G. A. Fiete, Phys. Rev. B **87**, 121113 (2013).
[10] M. Bercx, M. Hohenadler, and F. F. Assaad, Phys. Rev. B **90**, 075140 (2014).
[11] C. Hickey, P. Rath, and A. Paramekanti, Phys. Rev. B **91**, 134414 (2015).
[12] C. Hickey, L. Cincio, Z. Papić, and A. Paramekanti, Phys. Rev. Lett. **116**, 137202 (2016).
[13] D. Prychynenko and S. D. Huber, Physica B **481**, 53 (2015).
[14] J. He, Y.-H. Zong, S.-P. Kou, Y. Liang, and S. Feng, Phys. Rev. B **84**, 035127 (2011).
[15] W. Zheng, H. Shen, Z. Wang, and H. Zhai, Phys. Rev. B **91**, 161107 (2015).
[16] J. He, S.-P. Kou, Y. Liang, and S. Feng, Phys. Rev. B **83**, 205116 (2011).
[17] V. S. Arun, R. Sohal, C. Hickey, and A. Paramekanti, Phys. Rev. B **93**, 115110 (2016).
[18] M. Jarrell, T. Maier, C. Huscroft, and S. Moukouri, Phys. Rev. B **64**, 195130 (2001).
[19] T. Maier, M. Jarrell, T. Pruschke, and M. H. Hettler, Rev. Mod. Phys. **77**, 1027 (2005).
[20] A. Georges, G. Kotliar, W. Krauth, and M. J. Rozenberg, Rev. Mod. Phys. **68**, 13 (1996).
[21] R. Landig, L. Hruby, N. Dogra, M. Landini, R. Mottl, T. Donner, and T. Esslinger, Nature (London) **532**, 476 (2016).

[22] A. Amaricci, J. C. Budich, M. Capone, B. Trauzettel, and G. Sangiovanni, Phys. Rev. Lett. **114**, 185701 (2015).
[23] A. Amaricci, J. C. Budich, M. Capone, B. Trauzettel, and G. Sangiovanni, Phys. Rev. B **93**, 235112 (2016).
[24] M. Messer, R. Desbuquois, T. Uehlinger, G. Jotzu, S. Huber, D. Greif, and T. Esslinger, Phys. Rev. Lett. **115**, 115303 (2015).
[25] E. Gull, P. Werner, O. Parcollet, and M. Troyer, EPL **82**, 57003 (2008).
[26] E. Gull, P. Staar, S. Fuchs, P. Nukala, M. S. Summers, T. Pruschke, T. C. Schulthess, and T. Maier, Phys. Rev. B **83**, 075122 (2011).
[27] J. Imriška, E. Gull, and M. Troyer, arXiv:1509.08919 [Eur. Phys. J. B (to be published)].
[28] S. Sorella, Y. Otsuka, and S. Yunoki, Sci. Rep. **2**, 992 (2012).
[29] F. F. Assaad and I. F. Herbut, Phys. Rev. X **3**, 031010 (2013).
[30] N. D. Mermin and H. Wagner, Phys. Rev. Lett. **17**, 1133 (1966).
[31] P. C. Hohenberg, Phys. Rev. **158**, 383 (1967).
[32] Z. Wang and B. Yan, J. Phys.: Condens. Matter **25**, 155601 (2013).
[33] T. Fukui, Y. Hatsugai, and H. Suzuki, J. Phys. Soc. Jpn. **74**, 1674 (2005).
[34] In case of the discontinuities, the topological gap closes during the run of the self-consistency, for a nonconverged iteration.
[35] J. Wu, J. P. L. Faye, D. Sénéchal, and J. Maciejko, Phys. Rev. B **93**, 075131 (2016).
[36] W. Wu and A.-M. S. Tremblay, Phys. Rev. B **89**, 205128 (2014).
[37] The largest difference between the noninteracting dispersions of the two compared models is at the M points, $\sqrt{t^2 - 27\lambda^2} - t$, where this is the shift of the van Hove peaks in the noninteracting density of states.
[38] N. Paris, K. Bouadim, F. Hebert, G. G. Batrouni, and R. T. Scalettar, Phys. Rev. Lett. **98**, 046403 (2007).
[39] S. S. Kancharla and E. Dagotto, Phys. Rev. Lett. **98**, 016402 (2007).
[40] K. Bouadim, N. Paris, F. Hébert, G. G. Batrouni, and R. T. Scalettar, Phys. Rev. B **76**, 085112 (2007).
[41] H.-F. Lin, H.-D. Liu, H.-S. Tao, and W.-M. Liu, Sci. Rep. **5**, 9810 (2015).
[42] Z.-L. Gu, K. Li, and J.-X. Li, arXiv:1512.05118.
[43] T. I. Vanhala, T. I. Siro, L. Liang, M. Troyer, A. Harju, and P. Törmä, Phys. Rev. Lett. **116**, 225305 (2016).
[44] A. Liebsch, Phys. Rev. Lett. **111**, 029701 (2013).
[45] S. R. Hassan and D. Sénéchal, Phys. Rev. Lett. **111**, 029702 (2013).
[46] C. N. Varney, K. Sun, M. Rigol, and V. Galitski, Phys. Rev. B **82**, 115125 (2010).
[47] L. Wang, H. Shi, S. Zhang, X. Wang, X. Dai, and X. C. Xie, arXiv:1012.5163.
[48] C. N. Varney, K. Sun, M. Rigol, and V. Galitski, Phys. Rev. B **84**, 241105 (2011).
[49] A. Albuquerque, F. Alet, P. Corboz, P. Dayal, A. Feiguin, S. Fuchs, L. Gamper, E. Gull, S. Gurtler, A. Honecker, R. Igarashi, M. Korner, A. Kozhevnikov, A. Lauchli, S. Manmana, M. Matsumoto, I. McCulloch, F. Michel, R. Noack, G. Pawlowski, L. Pollet, T. Pruschke, U. Schollwock, S. Todo, S. Trebst, M. Troyer, P. Werner, and S. Wessel, J. Magn. Magn. Mater. **310**, 1187 (2007).
[50] B. Bauer, L. D. Carr, H. G. Evertz, A. Feiguin, J. Freire, S. Fuchs, L. Gamper, J. Gukelberger, E. Gull, S. Guertler, A. Hehn, R. Igarashi, S. V. Isakov, D. Koop, P. N. Ma, P. Mates, H. Matsuo, O. Parcollet, G. Pawlowski, J. D. Picon, L. Pollet, E. Santos, V. W. Scarola, U. Schollwock, C. Silva, B. Surer, S. Todo, S. Trebst, M. Troyer, M. L. Wall, P. Werner, and S. Wessel, J. Stat. Mech.: Theory Exp. (2011) P05001.